

# The MinPET diamond discovery technique

T Nemakhavhani<sup>1</sup>, D Unwuchola<sup>1</sup>, R C Andrew<sup>1</sup>, M N H Cook<sup>1</sup>, S H Connell<sup>1</sup> and S E Ballestrero<sup>1</sup>, U Uggerhøj<sup>2</sup>, S Pape Møller<sup>2</sup>, P Aggerholm<sup>2</sup>, N Hertel<sup>2</sup>, J A Swartz<sup>2</sup>

<sup>1</sup>University of Johannesburg, Auckland Park, South Africa.

<sup>2</sup>University of Århus, Århus, Denmark.

E-mail: shconnell@uj.ac.za

**Abstract.** MinPET is a technology for diamond discovery in rock, specifically, the online, high throughput, quantitative, 3D imaging of local carbon concentration distributions in kimberlite. In the MinPET process, a high-energy photon beam of some tens of MeV irradiates a kimberlite rock stream, exciting the Giant Dipole Resonance. This transmutes especially some of the light stable isotopes within the kimberlite to become transient positron emitters, or Positron Emission Tomography (PET) isotopes. PET imaging of the rock is performed in an online run-of-mine scenario after a hold hopper, which delays detection for 20 minutes. After this time, <sup>11</sup>C, which has the longest PET isotope lifetime, is the dominant PET isotope. All non-diamond sources of carbon have a much lower carbon concentration than diamond, or they are diluted and finely dispersed within the kimberlite. Diamond is therefore evidenced by reconstructing the 3D quantitative carbon density distribution map. This contribution reviews the current status of the R&D towards a Mine Test Unit and concludes the technology is ready for deployment for such a unit in a full scale run-of-mine context. The expectation is that the technology is ready for deployment as a mine-test-unit operating in a full scale run-of-mine context

## 1. Introduction

The MinPET process has an activation and a detection stage, as depicted schematically in Figure 1 below [1, 2, 3, 4]. The activation stage consists of irradiation with a high-energy photon beam. This beam is produced by bremsstrahlung of a 40 MeV electron beam incident on a tungsten converter and then subsequently on the kimberlite rock stream. A shower develops as the mixed radiation field progresses through these materials. PET isotopes are produced primarily by the  $(\gamma, n)$  transmutation reaction, although there are several others, such as  $(\gamma, p(n))$ ,  $(\gamma, \alpha(n))$  and  $(\gamma, xn)$  which also need to be considered. The  $(\gamma, n)$  reaction has a high cross section ( $\sim 8$  mb) in the region of the Giant Dipole Resonance ( $E_\gamma \approx 20 - 30$  MeV). This transmutes various atomic species within the kimberlite to become transient positron emitters, or PET isotopes. PET stands for Positron Emission Tomography, as in the medical diagnostic technique for functional bio-imaging. It turns out that PET isotopes are the dominant sources of activity after several minutes. After about 20 minutes, <sup>11</sup>C is the dominant PET isotope. PET imaging of the rock after this time delay corresponds to a 3D quantitative imaging of the internal carbon distribution. All non-diamond sources of carbon have a much lower carbon concentration than diamond, or they are diluted and finely dispersed within the kimberlite.

This is then a technique on which to base the intelligent sensor-based sorting of barren from diamondiferous kimberlite. The contrast ratio is about 10:1 for diamond as compared to wood, rubber, large carbonate particles and so on. Kimberlite contains carbonates, usually quantified as an amount of CO<sub>2</sub>. The fractional composition of this by weight is variable but a reference

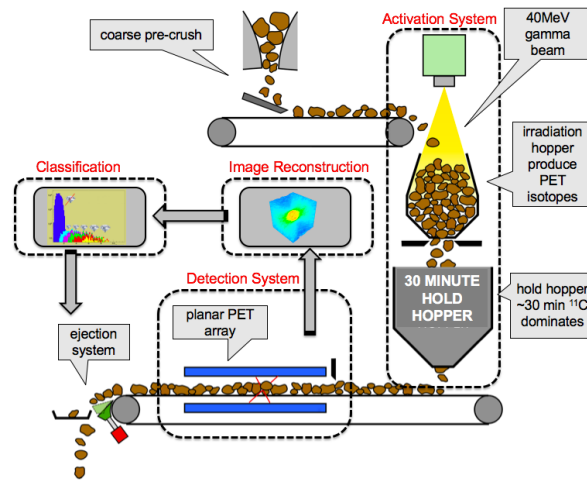


**Figure 1.** Schematic diagram of the MinPET process. Coarse crushed (<100 mm) kimberlite rock is irradiated with high energy photons. The hold hopper of ~20 min allows non-carbon PET activity to decay out (mostly the  $^{15}\text{O}$ ), leaving  $^{11}\text{C}$  as the main surviving PET isotope component. The planar PET detector array identifies diamond via hotspots in the 3D carbon concentrations.

case could be 5%. The contrast ratio for diamond in kimberlite would then be about 45:1. The concept is technologically demanding, as in a typical diamond mine, the rock throughput could be about 500 tons per hour, on a belt moving at 1 m/s, the detectors would have about 2s to acquire the image, and the decision based on the quantitative visualisation of a diamond should be available within about 20s. The concentration of diamond in kimberlite by weight varies from mine to mine, but typically it is just under a carat (0.2 g) per ton of kimberlite. Global production, as measured by the Kimberley Process Certification Scheme (KPCS), was 134-million carats in 2016 [5]. One therefore finds the crushing and processing of about 100 million tons of kimberlite rock per year, an unnecessary multi-billion dollar (barren) rock processing business. Normally the recovery of diamond is accomplished by a sequence of crushing and concentration operations. The concentration could be achieved by dense media separation, grease tables, dual energy X-ray transmission (XRT) and X-ray stimulated optical fluorescence (XRF). The early crushing to small rocks in these methods leads to diamond breakage. In addition they require substantial plant, they are not sufficiently efficient, they usually require a lot of water and lead to slimes dams. MinPET is therefore a potential disruptive technology. Diamond mining is expected to become more efficient, the recovered diamonds would suffer much less breakage, mining would be greener, mine life would be extended and sub-marginal mines could become competitive.

## 2. Full Dress Rehearsal, lab scale

A test of the performance of the MinPET technology requires the processes of activation, delay and then detection to be implemented on test samples of kimberlite rock spiked with diamond. Previous work has identified a benchmark dose for the case of a 40 MeV electron accelerator providing a beam current of 5 mA over a footprint of 1 m<sup>2</sup> to a belt of width 1 m moving at 1 m/s irradiating kimberlite rock with a throughput of 500 tons per hour. A detailed Geant4 [6, 7, 8] simulation is used to quantify the specific activity of various PET isotopes that is generated in this case for a reference kimberlite rock. In the simulation, the mixed radiation field that evolves is folded with the various nuclear cross sections for the processes mentioned above, in the evaluation of the specific PET activity. The benchmark dose producing this activity in a

reference sample of kimberlite leads to the definition of the MinPET dose and the MinPET specific activity. The benchmark MinPET detector here would be a planar detector array of  $2\text{ m} \times 1\text{ m}$  above and below the belt. The Geant4 simulation extends to detection and reconstruction of an event-by-event file of the lines of response (LoR). This then leads to the concept of the required MinPET detection capacity, which can successfully detect down to a given small diamond size within a given kimberlite rock size. The reference sizes here at the moment are a 4 mm diamond within a 100 mm particle of kimberlite containing 5% of carbon expressed as a weight percent of  $\text{CO}_2$ . It is necessary to specify these additional details as the first represents the signal activity, the second represents the amount of the systematic affects of scattering and attenuation for the annihilation 511 keV photons that affect the fidelity and number of the resulting LoRs, and the third relates to non-diamond carbon irreducible background.

When testing the performance of a lab-scaled MinPET system, it must be scaled in performance to a full run-of-mine MinPET system, which delivers an effective MinPET Dose, and generates the same specific activity in the kimberlite, and has a similar detection capacity, as the benchmark case described above. The differences in accelerator power and detection surface area are absorbed into adjustments to the throughput rate. In all, one seeks to have ultimately the same total number of LoRs that contribute to the image formation process, in the benchmark MinPET run-of-mine scenario as compared to the lab-scale Full Dress Rehearsal performance test scenario.

### *2.1. Activation*

There are very few accelerators world-wide with a capacity for 40 MeV electrons, which can be re-purposed for general irradiations. Our full dress rehearsal experiments were recently carried out at the electron injector microtron of the ASTRID storage ring of the ISA, Centre of Storage Ring Facilities at the Department of Physics in Århus University, Denmark [9]. This injector microtron has an electron beam energy of 100 MeV. A 2.5 mm stainless steel degrader and a 5 mm copper degrader were used to soften the beam energy. The average beam current was 17 nA. This is a much weaker beam (about  $3 \times 10^5$  times) than that envisaged in the benchmark MinPET specification. Irradiation times were increased from 1 s to 600 s to partially compensate for this effect. This can be considered a maximum irradiation time to avoid strong saturation effects considering the lifetimes of the relevant PET isotopes, specifically that of  $^{11}\text{C}$  which is 20 minutes. The Geant4 simulations then allowed a scaling factor to be determined relating the specific activity produced in the lab-scale measurements at Århus to the benchmark MinPET scenario.

### *2.2. Detection*

The MinPET lab-scale detection system has a dual planar array of BGO crystals set out with each plane comprising a matrix of 1024 pixels arranged in a  $32 \times 32$  pixel square of dimension  $20\text{ cm} \times 20\text{ cm}$ . The light is collected into Hamamatsu H8500 photomultipliers (PMs). The read-out system has been specially designed and commissioned by Net Instruments for the MinPET application. This system will be described later elsewhere. The data acquisition system proceeds from front end FPGAs on each PM control board, to an FPGA on the planar array which does the event building for its side of the LoR. This system is controlled by an on-board PC. A coincidence determination is made with essentially no latency via a separate communication between the two planes. A trigger signal is generated to ensure that the two planar arrays publish only coincidence events to a fast network, containing their own data for their side of the LoR. The acquisition software can then build the LoRs after matching events from each plane. From there the data can be visualised using ROOT [10] and further analysed and also stored for additional off-line analysis. The rate of passage of the rock in a run-of-mine MinPET

system is 1 m/s for a 2 m × 1 m area of dual planar detectors. These lab-scale detectors have a fraction of this area. The rate of passage through the detector was determined to be 1 cm/s, as explained in the next section. This longer detection time would compensate the smaller detector size and part of the uncompensated component of the weaker accelerator beam, which was not fully compensated for by the longer irradiation time mentioned above. These compensations also included other systematic considerations which have been mentioned already.

### 2.3. Integration

The integration of the Activation-Detection system together, to represent a scaled version of the benchmark MinPET activation and detection system, considers both the lower accelerator beam current and the smaller capacity of the current lab-scale PET detection system, among other differences. Essentially the lower beam current with a different mixed radiation field profile is partially compensated for by a longer irradiation time. The smaller detector system and the remaining uncompensated factor for the irradiation stage is compensated for by a longer count time in the detectors. This corresponds to a slower passage of the rock through the MinPET detector array. More precisely, the considerations mentioned are modelled in Geant4, and the lab-scale test is compared to the benchmark MinPET scenario in the context of the net number of LoRs produced and detected in each of the cases. An approximate analytic calculation of the effects of the considerations mentioned leads to a similar conclusion to the detailed Geant4 modelling. The Geant4 modelling has also been bench-marked to careful experiments of  $^{11}\text{C}$  activation by the same set-up as the Århus microtron, but where the activation was measured in absolute terms using efficiency-calibrated HPGe detectors. The Geant4 modelling of PET activity production by the Århus beam and the benchmark MinPET beam is therefore considered robust. In the results that follow, we therefore expect that the lab-scale experiments at Århus, with a weaker accelerator and small detector, but longer irradiation and count times, nonetheless correspond in terms of specific activation and detection efficiency to the benchmark scenario of a full run-of-mine MinPET scenario. That is to say, the results represent a test of MinPET corresponding to the throughput of a scaled up system capable of handling 500 tons per hour, and then discovering diamonds of a given size within a 100 mm particle of kimberlite where the carbon background as specified by  $\text{CO}_2$  concentration by weight is 5%.

## 3. Reconstruction

The reconstructions that are shown later represent processing of the event-by-event LoR data to form 3D images using the CUDA-enabled ASTRA package [11, 12, 13]. The implemented algorithm is the iterative maximum likelihood method [14, 15] to find the most likely 3D source distribution for PET activity that best corresponds to a set of recorded 2D projections. The 2D projections used are obtained by binning the LoR event-by-event data based on a carefully chosen set of polar and azimuthal angles. This is effectively a higher dimensional sinogram. The reconstructed 3D image is treated to consider the systematic effects of the spatial non-uniformity of the Århus microtron beam compared to the spatial extent of the rock profile, and also for the “Compton Wind” effect of the depth dependence of softening of the mixed radiation fields energy distribution. In this data, there is not yet a correction for scattering and attenuation of the 511 keV annihilation photons. Such corrections would increase the detail seen in the reconstructions.

## 4. Results

The results are presented as reconstructed PET images, where only a sectional slice of the full 3D data-set is shown. The images should be interpreted as maps of the PET activity, where the dominant emitter is carbon. Hotspots in the image identify a buried diamond. The slice is chosen at the position that intersects the enclosed diamond. The slice form of presentation is

chosen as the full 3D image may only be visualised via a digital medium. Figures 2 and 3 show the MinPET discovery images for a 2.9 carat diamond in the middle of a 100 mm cube, and a 5.0 carat diamond buried in the middle of a 74 mm diameter cylinder respectively.



**Figure 2.** MinPET discovery image for a 2.9 carat diamond buried in the middle of cube of kimberlite of side 100 mm (2.3 kg).

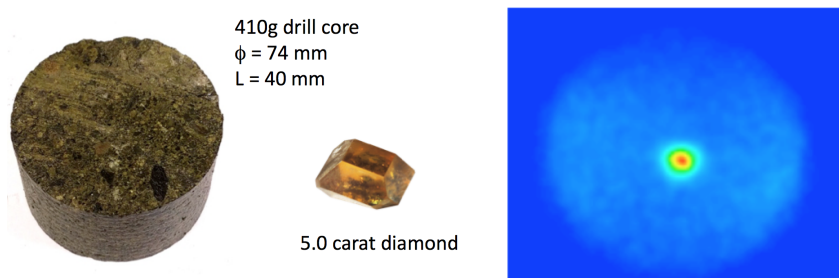


**Figure 3.** MinPET discovery image for a 5.0 carat diamond buried in the middle of cylinder of kimberlite of diameter 74 mm and length 40 mm (413 g).

Figure 4 shows the MinPET discovery image for a 10.3 carat diamond buried in the middle of calcite rock of length 150 mm. Calcite is a worst case scenario for MinPET as it has a high PET irreducible background. Its chemical formula is  $\text{CaCO}_3$ . The activation stage produces the PET isotopes  $^{12}\text{C}(\gamma, n)^{11}\text{C}$ ,  $^{16}\text{O}(\gamma, n)^{15}\text{O}$ ,  $^{16}\text{O}(\gamma, n\alpha)^{11}\text{C}$  and  $^{40}\text{Ca}(\gamma, np)^{38}\text{K}$ . The PET activity of a possible diamond has to be visualised against a background of the PET activity of all the calcite constituent elements that could be activated too.

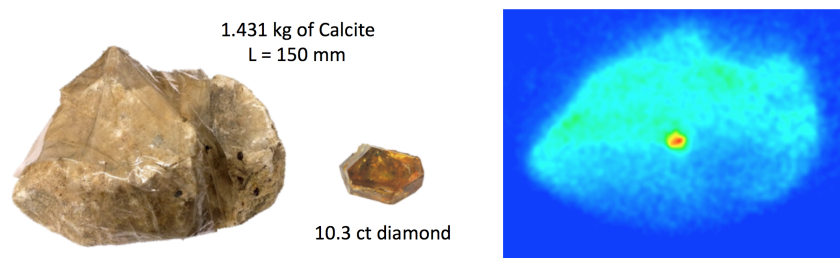


**Figure 4.** MinPET discovery image for a 10.3 carat diamond buried in the middle of calcite rock of length 150 mm (1.413 kg).

## 5. Conclusions

A Full Dress Rehearsal for the MinPET lab-scale technology demonstrator has been described. This means that the activation and detection stages are coupled and scaled to represent a

benchmark MinPET system capable of run-of-mine throughputs (500 tph). The data shown represent PET reconstructions of essentially carbon 3D spatial concentrations. The sizes of diamonds buried within rocks of specified types and sizes is given for each image, and these are similar scenarios to those found in a mining context. The clarity with which a diamond may be recognised within the images therefore is an indication of the performance of the MinPET process in the specified conditions. Currently MinPET can discover at least a 4 mm diamond in a 100 mm kimberlite or a 2 mm diamond in a 40 mm kimberlite, under the conditions described above. The expectation is that the technology is ready for deployment as a mine-test-unit operating in a full scale run-of-mine context.

## 6. Acknowledgements

The authors acknowledge financial support of the National Research Foundation (NRF) and the IAEA TC CPF Programme, as well as provision of accommodation by Resolution Circle and iThemba LABS.

## References

- [1] TSA Patent 2006/08025, ARIPO Patent AP/P/2006/003753 (covers Botswana, Namibia, Lesotho and Zimbabwe), Canadian Patent 2,559,516, Australian Patent 2005220403, Russia Patent 2006135960, India Patent 5365/DELNP/2006F
- [2] Ballestrero S et al 2010 *CERN-Proceedings-2010-001, Proceedings of the 12th INTERNATIONAL CONFERENCE ON NUCLEAR REACTION MECHANISMS Varenna (Italy), Villa Monastero, 15-19 June 2009* 589–602
- [3] Tchonang M, Cook M, Bornman F, Connell SH and Ballestrero S 2014 *Proceedings of SAIP2013: the 58th Annual Conference of the South African Institute of Physics, edited by Roelf Botha, Thulani Jili, ISBN: 978-0-620-62819-8*. 502–506 URL <http://events.saip.org.za>
- [4] Cook M, Tchonang M, Chinaka E, Bhamjee M, Bornman F and Connell SH 2015 *Proceedings of SAIP2014, the 59th Annual Conference of the South African Institute of Physics, edited by Chris Engelbrecht and Steven Karataglidis (University of Johannesburg, ISBN: 978-0-620-65391-6*. 479–484 URL <http://events.saip.org.za>
- [5] Kimberley Process Certification Scheme 2016 *Annual Global Summary: 2016, Production, Imports, Exports and KPC Counts* URL [https://kimberleyprocessstatistics.org/static/pdfs/public\\_statistics/2016/2016GlobalSummary.pdf](https://kimberleyprocessstatistics.org/static/pdfs/public_statistics/2016/2016GlobalSummary.pdf)
- [6] Agostinelli S et al (GEANT4 Collaboration) 2003 *Nucl. Instrum. Meth. A* **506** 250–303
- [7] Agostinelli S et al (GEANT4 Collaboration) 2006 *IEEE Transactions on Nuclear Science* **53** 270–278
- [8] Agostinelli S et al (GEANT4 Collaboration) 2016 *Nuclear Instruments and Methods in Physics Research A* **835** 186–225
- [9] Uggerhøj E 1994 *Le Journal de Physique IV* **4** C9–349
- [10] Brun R and Rademakers F 1997 *Nuclear Instruments and Methods in Physics Research Section A: Accelerators, Spectrometers, Detectors and Associated Equipment* **389** 81–86
- [11] van Aarle W, Palenstijn W J, Cant J, Janssens E, Bleichrodt F, Dabravolski A, De Beenhouwer J, Batenburg K J and Sijbers J 2016 *Optics express* **24** 25129–25147
- [12] van Aarle W, Palenstijn W J, De Beenhouwer J, Altantzis T, Bals S, Batenburg K J and Sijbers J 2015 *Ultramicroscopy* **157** 35–47
- [13] Palenstijn W, Batenburg K and Sijbers J 2011 *Journal of structural biology* **176** 250–253
- [14] Dempster A P, Laird N M and Rubin D B 1977 *J. Roy. Stat. Soc., Ser. B* **39** 1–38
- [15] Shepp L A and Vardi Y 1982 *IEEE transactions on medical imaging* **1** 113–122